Available online at www.sciencedirect.com

ScienceDirect

IFAC Papers Online CONFERENCE PAPER ARCHIVE

IFAC PapersOnLine 50-1 (2017) 14539–14544

Application of a Fractional Order Integral Resonant Control to increase the achievable bandwidth of a nanopositioner. ⋆

Andres San-Millan * **Vicente Feliu-Batlle** ** **Sumeet S. Aphale** ***

* *Instituto de Investigaciones Energeticas y Aplicaciones Industriales (INEI), Campus Universitario de Ciudad Real, 13071 Ciudad Real, Spain (e-mail: andres.sanmillan.rodriguez@gmail.com).*
** *Escuela Tecnica Superior de Ingenieros Industriales, Universidad de Castilla-La Mancha, Ciudad Real, 13071 Spain(e-mail: vicente.feliu@uclm.es)*
*** *Center for Applied Dynamics Research, School of Engineering, University of Aberdeen, Aberdeen, AB24 3UE, U.K., (e-mail: s.aphale@abdn.ac.uk)*

AbstractThis paper proposes a Fractional-order modification of the traditional Integral Resonant Controller named as FIRC. The fractional integral action utilised in the proposed FIRC is a simple, robust, and well-performing technique for vibration control in smart structures with collocated sensor-actuator pairs such as nanopositioning stages. The proposed control scheme is robust in the sense of being insensitive to spillover dynamics and maintaining closed-loop stability even in the presence of model inaccuracies or time-delays in the system. The experimental and simulated results have showed that the proposed FIRC can provide a closed-loop bandwidth which spans up to a 95.2% of the first resonant mode of the experimental system, thus improving the bandwidth achieved by classical integer-order IRC implementations.

Keywords: Fractional-order control; Smart structures; Piezoelectric Actuators; Strain Gauges; Robust control.

1. INTRODUCTION

Increasing the achievable bandwidth and thus the operating speed of scanning probe microscopes (SPMs) is a critical problem. Usually the scanning frequency of high-resolution SPMs is situated at around 1/100 to 1/10 of the first resonant mode Clayton et al. (2009). Since triangular waveforms are utilised to produce the raster scanning, control techniques that enable closed-loop flat band response for a wide range of frequencies are necessary to cope with the frequency spectrum of these waves (which is composed of all the odd harmonics of the fundamental frequency Lathi (2009)).

This bandwidth-related limitation to SPM operating speed motivates the number of emerging trends in control techniques aiming to damp the mechanical-induced residual vibrations and to satisfy the critical requirements of nanopositioning stages to provide fast and accurate scanning mechanisms for SPMs. Among these techniques can be found: resonant control Pota et al. (2002), integral resonant control (IRC) Aphale et al. (2007), Positive Position Feedback (PPF) Aphale et al. (2008), and Positive Velocity and Position Feedback (PVPF) Russell et al. (2016).

IRC has demonstrated a robust performance and versatility, however when compared to the rest of aforementioned controllers, Russell et al. (2016) showed that the IRC presents the smaller achievable bandwidth. This reduced bandwidth is produced because the IRC presents only three parameters to tune while needing four closed-loop poles to be placed. Consequently, all the poles cannot be placed arbitrarily and thus, there is only one valid value of the cutoff frequency for the equivalent Butterworth filter design Russell et al. (2016) (which is usually close to the half of the resonant frequency of the system). Because of the simplicity and robustness advantages of the IRC scheme, it would be desirable to find a way to increase the achievable bandwidth and at the same time keep the frequency response as flat as possible in order to not distort the references applied to the controlled system.

Fractional-order controllers are usually utilised to design very robust schemes by designing the phase margin of the closed-loop system Monje et al. (2008) and have been widely utilised in the control of smart structures where the vibrations are a major issue, Monje et al. (2007); Feliu-Talegon et al. (2016). This paper proposes a fractional-order implementation of the classical IRC scheme (FIRC), where the damping controller is designed

⋆ This work has been supported in part by the Spanish Agencia Estatal de Investigación (AEI) under project DPI2016-80547-R (Ministerio de Economía y Competitividad), in part by the European Social Fund (FEDER, EU) and in part by the Spanish scholarship FPU12/00984 of the FPU Program of the Ministerio de Educacion, Cultura y Deporte.

10.1016/j.ifacol.2017.08.2079

as in Namavar et al. (2014) to maximize the damping of the system, and the tracking controller is replaced by fractional-order integrator. This new implementation increases the number of available design parameters by one and facilitates increasing the achievable bandwidth while keeping the frequency response within the ±3dB band.

This paper is organised as follows: Section 2 presents the mathematical model for one axis of a piezoactuated nanopositioner. The integer and fractional-order IRC controllers (FIRC) are formulated in Section 3 and 4. Section 5 describes the experimental platform utilized in this work. Section 6 presents the simulations and analysis thereof to study the robustness and sensitivity of the proposed controller, and the experimental results and conclusions are presented in Sections 7 and 8 respectively.

2. DYNAMIC MODEL

The vibrational dynamic behavior of a flexure-hinge-guided piezo-actuated nanopositioning stage can be modelled by means of an infinite sum of second-order systems with lightly damped resonant modes:

$$G_M(s) = e^{-\tau s} \sum_{i=1}^{M} \frac{\sigma_i^2}{s^2 + 2\zeta_i \omega_i s + \omega_i^2} \tag{1}$$

where M denotes the number of modes of vibration considered in the transfer function and ideally $M \to \infty$, σ_i^2 corresponds to the gain of each mode of vibration, ζ_i is the damping ratio of each mode, ω_i is the natural frequency of vibration of each mode, and τ is the value of the time delay of the system.

The infinite number of modes of vibration and the delay in (1) makes controlling these systems a challenging task because of the infinite number of poles introduced by the infinite modes of vibration, and by the inherent system delay which can be modeled by the transcendental transfer function.

3. INTEGER-ORDER IRC CONTROL

The IRC controller as it was first proposed in Aphale et al. (2007) was applied to (1) without time delay and reverses the pole–zero interlacing of the collocated system $G(s)$ to zero–pole interlacing by adding a constant feed-through term d to the system. As a consequence the phase of the resulting transfer function lies between $0°$ and $-180°$. This modified system adds in positive feedback an integral controller, $C_d(s)$, which produces a substantial damping of the multiple resonant modes. Despite having proved to be very robust and broadly applicable to nanopositioning stages, this technique only provides damping to the resonant modes and does not provide any tracking necessary to compensate for the nonlinear hysteresis and creep effects introduced by the piezoelectric actuators. Consequently, the IRC is complemented with a simple tracking scheme $C_t(s)$ (usually an integral controller) to minimize the positioning errors introduced by these nonlinear effects Aphale et al. (2008). This composite damping and tracking control scheme is shown in Fig.1.

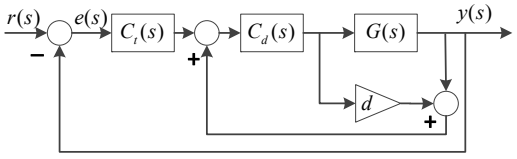

Figure 1. Block diagram for the traditional IRC damping controller in addition to integral tracking controller scheme.

The first approaches utilised to design the parameters of the IRC scheme were based on trial-and-error. The work of Namavar et al. (2014) presents the analytical relationships which relate the maximum damping achievable with the IRC and the value of the parameters of the controller. Additionally, key relationships between the feed-through term, the gains of the damping and tracking controller and the performance achieved are also postulated by means of an intensive search among the different combinations of the parameters and their effect over the bandwidth achieved.

Recently, new design rules which produce the optimal frequency response for tracking applications were presented in Russell et al. (2016). These rules provide a maximally flat band response with unity gain which roll-off at frequencies beyond the desired bandwidth, and consist on placing the closed-loop poles of the controlled system in the pattern of a Butterworth filter, i.e. equally spaced on a circle with radius equal to the natural frequency on the filter. However, this technique presents two main drawbacks: a) It was demonstrated in Russell et al. (2016) that the radius of the circle along the closed-loop poles are distributed can only take a fixed value which is smaller than the resonant frequency of the system, (which means that only a relatively small bandwidth can be achieved) and b) Despite the system described in (1) can be aptly simplified to a single-mode second-order model, the effect of the delay cannot be neglected, thereby making the methodologies proposed in Namavar et al. (2014) and Russell et al. (2016) inapplicable in case of systems with delay. These drawbacks are overcome using the fractional-order IRC design as proposed in the following section.

4. FRACTIONAL-ORDER CONTROL SCHEME

Due to the substantial spacing between consecutive resonant modes, the system described in (1) can be simplified to a single-mode second-order model where $M = 1$, which leads to:

$$G(s) = e^{-\tau s} \frac{\sigma^2}{s^2 + 2\zeta\omega s + \omega^2} \tag{2}$$

where the index $M = 1$ has been omitted for the sake of clarity. Considering the system of (2), the fractional-order implementation of the IRC scheme presents the closed-loop block diagram shown in Fig.1, where each block has the following expressions:

$$C_t(s) = \frac{K_i}{s^\alpha},\ C_d(s) = \frac{K_d}{s} \tag{3}$$

where K_i is the gain of the tracking controller, α is the fractional exponent, K_d is the gain of the damping controller and d is the feed-through term. It can be seen that, considering $\alpha = 1$, the traditional IRC scheme is obtained, and the maximally flat band response, i.e. the Butterworth filter response can be achieved by placing the closed-loop poles equally spaced on a circle of radius ω_B.

However for values of $0 < \alpha < 1$ the extension of the concept of analog Butterworth filter and its maximally flat-band response is more complex and, as it was shown in Acharya et al. (2014), the poles of these fractional-order Butterworth filters need to be placed in very specific locations along Q Riemann sheets (where Q is related to the number of decimals of the fractional order of the filter). If we study the closed-loop transfer function of the system (even in the simplest case where delay is negligible, or τ=0) the denominator of the closed-loop transfer function of the system takes the following form:

$$M(s)_{den} = s^{3+\alpha} + s^{2+\alpha}(2\zeta\omega - d \cdot K_d) + s^{1+\alpha}(\omega^2 - 2\zeta\omega d K_d) - s^{\alpha} K_d(d\omega^2 + \sigma^2) + K_d K_i \sigma^2 \quad (4)$$

The restriction imposed in Acharya et al. (2014) determines very definite conditions on the structure of the denominator of fractional-order Butterworth filters, which cannot be satisfied by (4). It is important to note that since this condition cannot be satisfied in the simplest case without time delay, the case with an arbitrary time delay τ will be impossible to satisfy as well.

However in this paper we are looking for a compromise between increasing the maximum achievable bandwidth and keeping a flat in-band response. In our case this is achieved by following a two step procedure: First the parameters of the damping controller of the IRC, K_d and d, are designed following the equations provided in Namavar et al. (2014) so that the damping provided by the controller is maximized, and once these parameters have been computed, the parameter of the tracking controller of the IRC, K_i, is designed by numerical optimization for each value of α. In order to maximize the achievable bandwidth and to keep a flat-band response inside the ±3 dB band, the following optimisation criteria and restrictions are utilised:

- The maximum bandwidth, ω_{bw}, is defined as the lowest frequency at which the -1dB line is crossed by the magnitude response of the closed loop system.
- The maximum allowed amplitude of the band pass ripple, δ_{max}, is defined as the maximum value reached by the magnitude response of the closed loop system for frequencies below ω_{bw}.
- The closed loop system must be stable.

It is important to note that for practical purposes (as inaccuracies in the parameters of the identified system), the optimisation procedure utilises the ±1dB band as admissibility criterion (δ_{max}=1). Once the goals and restrictions of the problem have been set, the design procedure is performed by following these steps:

(1) The nanopositioning stage is identified and the numerical values of the parameters of the first mode of vibration,σ, ω and ζ, are obtained.
(2) The following equations from Namavar et al. (2014):

$$d = -2\frac{\sigma^2}{\omega^2}, K_d = \frac{1}{|d|}\left(\omega\sqrt{\frac{\omega}{\sqrt{\omega^2 + \sigma^2/d}}}\right) \quad (5)$$

are utilised to design the parameters of the damping controller of the IRC that prove the maximum damping to the system.
(3) The value of α is varied in the interval [1,0] in decrements of $\Delta\alpha$=0.1.
(4) For each new value of α the value of K_i is obtained by using the gradient method to maximize ω_{bw}. It is important to note that the frequency response of the closed-loop system utilised in the optimisation procedure is computed considering the complete model (including the delay) showed in (2)
(5) If a new value of α cannot lead to a feasible solution (due to instability of because it cannot fulfill the restriction of δ_{max}) the value of α is considered as unreachable.

The application of an optimisation procedure to the design of a fractional-order filter is not new. In Matos and Ortigueira (2010) and Freeborn et al. (2015) differential evolution and nonlinear least squares optimization algorithms were utilised respectively to adjust the parameters of a fractional-order filter to approximate the response of an integer order filter. In our case, however, we are trying to maximize the achievable bandwidth under the well-know criterion of the ±3 dB. In it important to note that the design considers a ±1 dB band, but the actual performance is evaluated following the ±3 dB criterion.

5. EXPERIMENTAL SETUP AND SYSTEM IDENTIFICATION

The fractional-order control scheme proposed in this paper was tested on a two-axis nanopositioner with a flexure-based XY serial mechanism driven by two PZT stacks as seen in Fig.2. Two piezoelectric amplifiers configured to provide a gain factor of 20 times the control signal and a bias of 100 V are utilised to drive the two PZT stacks (only the $x-$axis was utilised to perform the experiments presented in this work, while control signal of the $y-$axis was set 0V to mimic a realistic platform operation). The cross-coupling between the two axes of the nanopositioner is -40 dB, thus making it feasible to treat each axis as being decoupled from the other. In our experimental setup the translational motion along the $x-$axis is measured by a Microsense 4810 capacitive displacement sensor and a 2805 measurement probe with a sensitivity of 5 μm/V. Additionally, a PCI-6621 data acquisition card from National Instruments installed on a PC running the Real-Time Module from LabVIEW is used to interface between the experimental platform and the control design. The PC utilized is an OPTIPLEX 780 with an Intel(R) Core(TM)2 Duo Processor running at 3.167 GHz and equipped with 2GB of DDR3 RAM memory.

The nanopositioner was identified by using the small signal frequency response function (FRF) in the range [0,1800] Hz in order to capture the first four resonance modes of the platform (at 716.2, 1235.5, 1294, and 1578 Hz) and to quantify the delay (which can be seen as a linear term in the phase response of the system). The procedure utilised to obtain the transfer function of the system consists of two

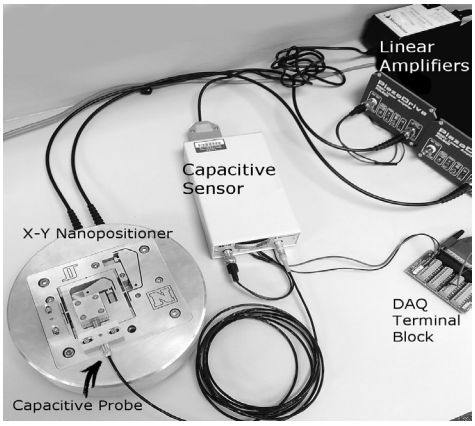

Figure 2. Two-axis serial kinematic nanopositioner.

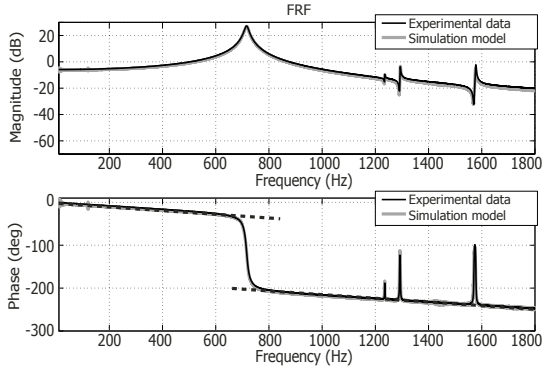

Figure 3. FRF of the x-axis of the experimental platform measured from the input voltage to output displacement.

steps: first the resonance modes of the transfer function of the system were obtained by using the subspace based modelling technique described in McKelvey et al. (1996), and then the delay was adjusted by minimizing the root-mean-square error (RMSE) of the phase response. The transfer function identified was:

$$G_4(s,\tau) = \frac{1.024\times10^7 e^{-\tau s}}{s^2+99s+2.025\times10^7} + \frac{10000e^{-\tau s}}{s^2+7.76s+6.026\times10^7} + \frac{62500e^{-\tau s}}{s^2+13.01s+6.61\times10^7} + \frac{122500e^{-\tau s}}{s^2+15.86s+9.83\times10^7} \quad (6)$$

where: τ=115 μs. The identified model accurately captures the first four resonant modes of the platform and accounts for the delay in the system, as shown in Fig.3. However, only the first resonant mode is utilised to design the proposed control scheme whereas the remaining modes of vibration are utilised only to validate the stability of the control scheme and its robustness to spillover effects.

The fractional exponent of the proposed controller is implemented in the experimental platform by using the following expression:

$$C_t(s) = \frac{K_i}{s^\alpha} = \frac{K_i}{s}s^\beta \quad (7)$$

where β=1−α. And by using the Grünwald-Letnikov (GL) definition of the discretized fractional operator Vinagre et al. (2000), and the short memory approximation Podlubny (1998),as follows:

$$y_c(t) = T_s^\beta \sum_{j=0}^{N-1}(-1)^j \binom{\beta}{j} f(t-jT_s); \quad (8)$$

where $f(t)$ is the input to the block s^β and is the integral of the error signal $(r-y)$ multiplied by K_i, $y_c(t)$ is its output, N=200 is the number of terms involved in the discrete convolution, T_s is the sampling time and the combinatorial has been generalised in the following respect:

$$\binom{\beta}{j} = \frac{\beta(\beta+1)...(\beta-j+1)}{j!}. \quad (9)$$

6. SIMULATED RESULTS

Simulations are performed using two different models of the identified experimental platform. On the one hand, a simple second order model corresponding to the first mode of vibration of (6) was utilised to design the parameters of the FIRC scheme by following the optimization procedure proposed in Section 4. On the other hand, once the optimization procedure was completed and the parameters of the FIRC were designed for the different values of α, these controllers were simulated in a closed-loop scheme where the four modes of vibration of (6) were included. This complete model of the nanopositioner was utilised in order to verify the stability of the designed controllers even in the presence of high-frequency modes that were not considered in the design stage. In order to verify the performance of the proposed fractional order IRC scheme different designs of the IRC were implemented in simulation and in the experimental system.

- Butterworth Pattern-based IRC Design:
  The first controller analysed in this paper is the classical integer-order IRC designed by using the methodology proposed in Russell et al. (2016) to place placing the closed-loop poles of the system (considering the delay negligible) as in a Butterworth filter. This design present the smaller bandwidth because it was conceived to be applied to systems with a negligible delay.
- Maximum damping IRC Design:
  The first step of the design procedure proposed in this paper is to design the integer-order IRC by using the methodology proposed in Namavar et al. (2014) tuning in first place the parameters K_d and d to maximize the damping provided by the controller by using the relationships (5), and then designing the tracking gain K_i via simulations to maximize the achievable bandwidth (in this case it was considered the delay of the system in the simulations utilised to design the controller).
- Fractional order IRC Design:
  The methodology proposed in this paper is utilised to design the fractional-order implementation of the IRC scheme for a number of different values of α in order to illustrate the effect of the change of the fractional exponent over the achievable bandwidth. The parameters of the different controllers and the

achieved bandwidths can be seen in Table 1. It is important to note that the case α=1 corresponds to the integer-order IRC named as the "Maximum damping IRC Design". It is also important to note that the optimisation procedure showed that the values of $\alpha \in$[0,0.5] where unreachable under the restrictions of the optimisation procedure (particularly the restriction δ_{max}=1).

α	K_i	K_d	d	BW$_{Sim.}$ (Hz)	BW$_{Exp.}$ (Hz)
1.0	418.66	8724.17	-0.729	208.6	223
1.0	1000	5291.39	-1.011	268.8	274.8
0.9	680	5291.39	-1.011	570.8	516.2
0.8	330	5291.39	-1.011	615.8	588.4
0.7	150	5291.39	-1.011	638	623
0.6	70	5291.39	-1.011	662.6	681.8

Table 1. Parameters of the regulators utilised, and bandwidth obtained in simulation and experimentally.

Considering the results showed in Table 1, it can be seen that the optimal value of α corresponds to 0.6 since it produces the maximum bandwidth achievable.

6.1 Robustness analysis

As stated in the introduction, the main advantage of the fractional-order controller is its ability to increase the phase margin robustness of the closed-loop system. The tracking scheme $C_t(s)$ of the FIRC can be written as:

$$C_{CPE}(s) = C_t(s) = K_i s^{\alpha}, \tag{10}$$

where $\alpha < 0$. It is clear that this transfer function corresponds to the well-known constant phase element (CPE) Cole (1933).This transfer function has a frequency response with a constant phase between the entire range of frequencies $0 < \omega < \infty$, and allows regulator designs with desired phase margins. In order to show the robustness of the regulators parametrized in Table 1, the Nyquist plots using the different regulators were plotted (considering the four vibration modes of the system) to obtain the phase margin Φ_M and gain margin M_g, and the values of the frequencies at these points (ω_c and ω_g). These values are shown in Table 2.

α	$\Phi_M(^\circ)$	$\omega_c(Hz)$	$M_g(dB)$	$\omega_g(Hz)$
1	56.38	155	8.86	430
0.9	53.17	214	5.86	469
0.8	62.17	214	5.53	506
0.7	75.06	195	5.58	539
0.6	87.16	180	5.29	570

Table 2. Representative points of the Nyquist diagram for the different controllers designed depending on α.

From the results shown in Table 2, it is clear that despite the value of phase margin is increased as the value of α is decreased, the gain margin is maintained approximately constant for all the designed controllers (which implies increased stability robustness and damping robustness), and this gain margin is also guaranteed for all the vibration modes, thereby avoiding the detrimental effects due to unmodelled spillover dynamics.

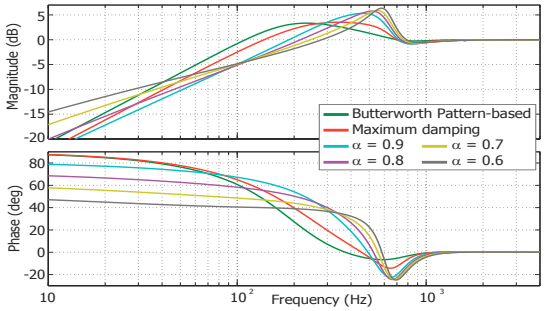

Figure 4. Bode's sensitivity integrals and phase responses for the sensitivity function $S(s,\tau) = \frac{e(s)}{r(s)}$ for all the controllers analysed considering a delay of $\tau = 115\mu s$

6.2 Impact of the fractional exponent on the sensitivity function

The proposed control scheme is a fractional extension of the integer-order IRC. It is therefore important to discuss the impact of the fractional exponent on the behavior of the controlled system. The most straightforward method is to study the sensitivity of the controlled system.

Upon studying Fig. 1, the closed-loop sensitivity function of the FIRC control scheme is found to be:

$$S(s,\tau) = \frac{e(s)}{r(s)} = \frac{1-C_d(s)(G_4(s,\tau)+d)}{1+C_d(s)(G_4(s,\tau)(C_t(s)-1)-d)} \tag{11}$$

Studying the sensitivity of the system allows also to keep in mind the performance limits of any designed control scheme. The fractional exponent increases the sensitivity at low frequencies (a common issue with fractional-order controllers is that decreasing the fractional exponent results in a slower convergence to the steady state). However as the integral of the log of the magnitude of the sensitivity has to remain equal to zero due to the so-called "Waterbed effect" Stein (2003), the sensitivity at high frequencies is decreased, and thus the frequency where the unity sensitivity is crossed (denoted as Ω_0) is increaased.

The Bode's sensitivity integrals for all the controllers when considering a delay of $\tau = 115\mu s$ (associated with the sampling time of $50\mu s$ of the experimental platform) are displayed in Fig. 4. By observing the Bode's sensitivity integral of all the controllers, it can be observed that each of the analysed controllers increases the value of Ω_0 reached by the previous one, i.e. the Butterworth-base design provides $\Omega_0 = 110.7$ Hz, the "Maximum damping IRC Design" provides $\Omega_0 = 138$ Hz, and the FIRC implementations of α=0.9, 0.8, 0.7 and 0.6 provides $\Omega_0 = 190$ Hz, 215 Hz, 242 Hz, and 284 Hz respectively.

This increase in Ω_0 from one controller to another, means that each controller increases the range of frequencies where the sensitivity function is lower than unity, and thus makes that controller more robust to external high-frequency disturbances.

7. EXPERIMENTAL RESULTS

The control schemes designed in Section 6 were evaluated on the two-axis serial kinematic nanopositioner detailed in Section 2. The performance of the different control schemes

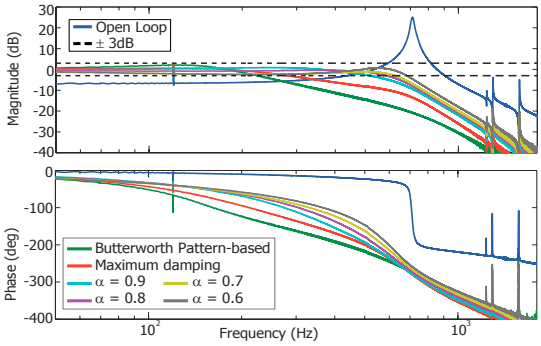

Figure 5. Open loop and closed-loop frequency response for the different controllers designed. Experimental results.

were evaluated in terms of achievable bandwidth, considering the ±3dB criterion. The experimental frequency response for the different controllers designed are showed in Fig. 5, and the numerical values of the different bandwidths achieved experimentally can be seen in the last column of Table 1.

It can be seen that there is a good agreement between the simulated and the experimental results, and that the proposed control scheme deliver a superior performance when compared with classical design techniques such as the Butterworth-based design (because these techniques do not take into account the effect of the delay present ion the system). Additionally it can be seen that if we attend to the results provided by the fractional-order controllers (in which all the cases have been designed considering the effect of the delay), it can be seen that the lower values of the fractional exponent provide the greater bandwidth achievable by the platform, providing in all the cases stable and robust closed-loop responses.

8. CONCLUSION

This paper proposes a fractional-order modification of the classical Integral Resonant Control (IRC), where a fractional-order integrator is utilised in the control loop devoted to tracking control. The addition of the fractional exponent provides an extra degree of freedom in the design of the controller that allows an increase in the achievable closed-loop positioning bandwidth while keeping a flat passband response within the ±3dB. The proposed control scheme demonstrated an increase of up to a 205.74% in the achievable bandwidth of the system compared with the traditional IRC controller without delay compensation, and up to a 143.5% when compared with integer-order techniques which take into account the delay of the system such as the Maximum damping IRC Design. The proposed fractional-order implementation has demonstrated its ability to provide a bandwidth which spans up to a 95.2% of the first resonant mode frequency of the experimental system, and that lower values of α lead to higher bandwidth but lower speed of convergence to steady state.

REFERENCES

Acharya, A., Das, S., Pan, I., and Das, S. (2014). Extending the concept of analog butterworth filter for fractional order systems. *Signal Processing*, 94, 409 – 420.

Aphale, S.S., Bhikkaji, B., and Moheimani, S.O.R. (2008). Minimizing scanning errors in piezoelectric stack-actuated nanopositioning platforms. *IEEE Transactions on Nanotechnology*, 7(1), 79–90.

Aphale, S.S., Fleming, A.J., and Moheimani, S.O.R. (2007). Integral resonant control of collocated smart structures. *Smart Materials and Structures*, 16(2), 439.

Clayton, G.M., Tien, S., Leang, K.K., Zou, Q., and Devasia, S. (2009). A review of feedforward control approaches in nanopositioning for high-speed spm. *Journal of Dynamic Systems, Measurement, and Control*, 131(6), 061101.

Cole, K.S. (1933). Electric conductance of biological systems. In *Cold Spring Harbor symposia on quantitative biology*, volume 1, 107–116. Cold Spring Harbor Laboratory Press.

Feliu-Talegon, D., San-Millan, A., and Feliu-Battle, V. (2016). Fractional-order integral resonant control of collocated smart structures. *Control Engineering Practice*, 2016, 14.

Freeborn, T., Maundy, B., and Elwakil, A.S. (2015). Approximated fractional order chebyshev lowpass filters. *Mathematical Problems in Engineering*, 2015, 7.

Lathi, B. (2009). *Linear Systems and Signals*. The Oxford series in electrical and computer engineering. Oxford University Press.

Matos, C. and Ortigueira, M.D. (2010). *Fractional Filters: An Optimization Approach*. Springer Berlin Heidelberg.

McKelvey, T., Akcay, H., and Ljung, L. (1996). Subspace-based multivariable system identification from frequency response data. *IEEE Transactions on Automatic Control*, 41(7), 960–979.

Monje, C.A., Ramos, F., Feliu, V., and Vinagre, B.M. (2007). Tip position control of a lightweight flexible manipulator using a fractional order controller. *IET Control Theory Applications*, 1(5), 1451–1460.

Monje, C.A., Vinagre, B.M., Feliu, V., and Chen, Y. (2008). Tuning and auto-tuning of fractional order controllers for industry applications. *Control Engineering Practice*, 16(7), 798 – 812.

Namavar, M., Fleming, A.J., Aleyaasin, M., Nakkeeran, K., and Aphale, S.S. (2014). An analytical approach to integral resonant control of second-order systems. *IEEE/ASME Transactions on Mechatronics*, 19(2), 651–659.

Podlubny, I. (1998). *Fractional differential equations: an introduction to fractional derivatives, fractional differential equations, to methods of their solution and some of their applications*, volume 198. Academic Press.

Pota, H.R., Moheimani, S.O.R., and Smith, M. (2002). Resonant controllers for smart structures. *Smart Materials and Structures*, 11(1), 1–8.

Russell, D., San-Millan, A., Feliu, V., and Aphale, S.S. (2016). Butterworth pattern based simultaneous damping and tracking controller designs for nanopositioning systems. *Frontiers in Mechanical Engineering*, 2(2).

Stein, G. (2003). Respect the unstable. *IEEE Control Systems*, 23(4), 12–25.

Vinagre, B.M., Podlubny, I., Hernandez, A., and Feliu, V. (2000). Some approximations of fractional order operators used in control theory and applications. *Fractional Calculus and Applied Analysis*, 3(3), 231–248.